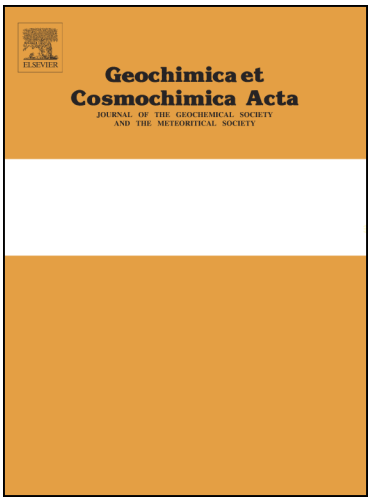

SO_2 scrubbing during percolation through rhyolitic volcanic domes

Ana S. Casas, Fabian B. Wadsworth, Paul M. Ayris, Pierre Delmelle, Jérémie Vasseur, Corrado Cimarelli, Donald B. Dingwell

PII: S0016-7037(19)30230-3
DOI: https://doi.org/10.1016/j.gca.2019.04.013
Reference: GCA 11208

To appear in: *Geochimica et Cosmochimica Acta*

Received Date: 18 May 2018
Revised Date: 20 February 2019
Accepted Date: 10 April 2019

Please cite this article as: Casas, A.S., Wadsworth, F.B., Ayris, P.M., Delmelle, P., Vasseur, J., Cimarelli, C., Dingwell, D.B., SO_2 scrubbing during percolation through rhyolitic volcanic domes, *Geochimica et Cosmochimica Acta* (2019), doi: https://doi.org/10.1016/j.gca.2019.04.013

SO_2 scrubbing during percolation through rhyolitic volcanic domes

Ana S. Casas[1], Fabian B. Wadsworth[2], Paul M. Ayris[1], Pierre Delmelle[3], Jérémie Vasseur[1], Corrado Cimarelli[1], Donald B. Dingwell[1]

[1]Earth and Environmental Sciences, Ludwig-Maximilians-Universität, Theresienstr. 41, 80333 Munich, Germany. [2]Earth Sciences, Durham University, Durham, DH1 3LE, U.K. [3]Earth and Life Institute, Université catholique de Louvain, Croix du Sud, 2 bte L7.05.10, B-1348 Louvain-la-Neuve, Belgium.

Corresponding author: anasilvia.casas@min.uni-muenchen.de

Accurate estimates of the atmospheric impacts of large eruptions on the environment are complicated by a paucity of models for gas-magma or gas-rock interactions that can occur in the subsurface. It is in these environments that high-temperature scavenging of magmatic gases, degassed during eruption, may play a major role, resulting in significant time-dependence of the bulk gas budget of the major erupted volatile species. Recent experimental work has identified the principal mechanisms involved in high-temperature scavenging in SO_2 and HCl-dominated gas environments, but has neglected the effect of humidity and in-dome gas-magma reactions. Here we present scaled experimental results for the scavenging potential in SO_2-H_2O mixtures using glassy rhyolitic particles above the acid dew point at 200-800 ºC. First, we reproduce previous results for anhydrous SO_2 scavenging. Such scavenging is accommodated by the growth of $CaSO_4$ crystals on the ash surface and limited by the temperature- and ash-size dependent diffusion of Ca^{2+} to the surface of the ash. Subordinate concentrations of Na_2SO_4 and potassium-bearing salts also grow on the ash surfaces. Na^+ and K^+ diffusion appear to be the limiting mechanisms for the formation of these salts, but once the bulk glass network is relaxed and equilibrates oxidation state above ~600 ºC, the diffusion of these cations is inhibited by charge compensation with Fe^{3+}. In SO_2-H_2O mixed-gas atmospheres, the diffusion of Ca^{2+} appears unaffected by the activity of H_2O on the ash surface. In contrast, the diffusion of Na^+ and K^+ toward the ash surface is enhanced. We speculate that this occurs by alkali exchange with inward diffusing H^+. In hydrous atmospheres, the diffusion of Na^+ and K^+ is also markedly less at the threshold oxidation temperature. This oxidation temperature is reduced to lower values as the water activity at the surface is increased by increasing the partial pressure of H_2O. Taken together, these results

enable the exploration of scenarios for in-dome processes where either open-system or batch outgassing prevails through fractures filled with populations of welding volcanic ash. Such scenarios predict that a large fraction of the SO_2 flowing through the ash-filled fracture networks may be scavenged in permeable fractured domes, which act as scrubbing filters, potentially explaining some unexpectedly low SO_2 emissions from rhyolitic dome-forming eruptions.

1. INTRODUCTION

Subaerial volcanic explosive eruptions release buoyant plumes of ash particles and magmatic volatiles into the atmosphere. Being subject to large temperature and compositional gradients upon air entrainment, eruption plumes are affected by various heterogeneous interactions. In particular, the common occurrence of sulphate and halide salts on ash can be attributed to gas molecule adsorption to ash surfaces, followed by several temperature-dependent reactions (Delmelle et al., 2007; Óskarsson, 1980; Rose, 1977). Besides sequestering magmatic volatiles (i.e., S, Cl and F), the surficial salt compounds modify the reactivity of airborne ash (Maters et al., 2017) and can subsequently dissolve and release an array of chemical elements upon contact of ash with water in receiving environments, potentially impacting terrestrial and aquatic ecosystems (Ayris and Delmelle, 2012).

While the precise reaction pathways by which sulphate and halide salts form on ash are not fully elucidated, Ayris et al. (2013; 2014) highlighted the significance of SO_2 and HCl gas removal (or scavenging) by ash in the hot core of large volcanic plumes and the shallow subsurface. According to these authors, in some end-member high temperature (800 °C) subaerial conditions of very large eruptions, up to 0.73 mass fraction of erupted SO_2 can be removed from the plume by formation of soluble salts, grown on the ash particle surfaces. A three-stage mechanism is invoked to explain SO_2 scavenging or "sequestration" by volcanic ash at high temperature: (1) SO_2 molecules are adsorbed onto reactive sites of freshly fragmented ash surfaces, (2) at the Ca-O surface sites, SO_2 undergoes temperature- and redox state- dependent reactions resulting in $CaSO_4$ growth, and (3) diffusion of CaO in the glass matrix proximal to the surface resulting from the concentration gradient triggering time- and temperature-dependent continued growth of $CaSO_4$. Thus, at times longer than a critical adsorption

time, SO_2 gas scavenging by ash at high temperature is dominantly limited by the diffusivity of cations required for the growth of salt deposits.

Active, passively degassing lava domes may offer ample opportunities for high-temperature SO_2 gas-ash interaction. There is evidence that rhyolitic volcanic domes and shallow conduits are heavily fractured (Tuffen et al., 2003) and that these fractures are dominant permeable outgassing pathways (Castro et al., 2012), especially during dome formation. Such systems are likely to be close to open-system (Castro et al., 2014; Castro et al., 2012), implying a decoupling between the gas phase and the melt-crystal suspension, and producing conditions for back-reactions (e.g., Schipper et al., 2015), including high-temperature gas scavenging. Yet, the significance of gas scavenging in-conduit or in-dome for volatile budgets is not clear. Importantly, rhyolitic lava domes are typically characterized by water-rich gas emissions (Giggenbach, 1996; Textor et al., 2004; Symonds et al., 1994) and the effect of water on SO_2 adsorption and reaction on ash surfaces also needs to be investigated.

Here we describe the results of a series of laboratory experiments in which natural rhyolitic glass was treated with SO_2-Ar and SO_2-H_2O-Ar gas mixtures for diverse time- and temperature series, using the Ash-Gas Advanced Reactor (Ayris et al. 2015). The objective of our study was to investigate the effects that grain size distribution, temperature, exposure time, and humidity can exert on SO_2 scavenging by rhyolitic glasses. These results differ from those of Ayris et al. (2013) in two important ways: (1) we cover the full range of parameters including a range of grain sizes and timescales, and (2) we include a determination of the effect of water on the process. Finally, scaling of our results allows us to evaluate the scavenging potential of the 2008 rhyolitic dome at Volcán Chaitén, Chile.

2. BACKGROUND TO HIGH-TEMPERATURE SCAVENGING MECHANISMS

Óskarsson (1980) identified the temperature-dependent nature of scavenging, recognising three temperature-dependent spatial zones, where ash-gas interactions occur: (1) a salt formation zone at magmatic temperatures, (2) a surface adsorption zone at temperatures above 700 °C and (3) a condensation zone at temperatures below ~338 °C. More recently, surveying adsorption rates across a range of volcanic glass compositions, Ayris et al. (2013) demonstrated that high-temperature SO_2 scavenging can produce rapid and significant sequestration of SO_2 mass fractions under an SO_2-air (1%,

70 mol.%, [He balance]) atmosphere. They showed that, at temperatures in excess of 600°C, conditions yield considerable scavenging of SO_2. Moreover, they identified Ca^{2+} diffusion from the glass matrix to the surface as the parameter limiting SO_2 scavenging rates at high temperature regimes. Ayris et al. (2014) confirmed that cation diffusion within the ash particles also limits the uptake of HCl gas on ash, however for rhyolitic compositions; HCl was much less reactive than SO_2.

Favorable adsorption of SO_2 onto the Ca-O ash surface sites was observed by Ayris et al. (2013), likely leading to $CaSO_3$ formation. The experiments described in Ayris et al. (2013) were performed in SO_2-air mixtures (see below). Further oxidation reactions are expected to occur depending on the thermal stability of $CaSO_3$, as described by Wieczorek-Ciurowa, (1992):

$$\left.\begin{array}{l} CaO + SO_2 = CaSO_3 \\ CaSO_3 + 0.5O_2 = CaSO_4 \end{array}\right\} \quad \sim 200 - 600°C$$

$$4CaSO_3 = 3CaSO_4 + CaS\} \quad 600 - 900°C$$

The high temperature reaction of SO_2 gas with glass to form $CaSO_4$ is preceded by adsorption, but salt growth is driven by subsequent Ca^{2+} diffusion towards the particle surface. Therefore, in what follows we use the term "scavenging" to refer to the complete process from adsorption to salt-growth.

3. EXPERIMENTAL MATERIALS AND METHODS

3.1 Sample characterisation and preparation

We used a rhyolitic composition represented by a crystal-free obsidian emplaced at Hrafntinnuhryggur, Krafla volcano, Iceland. The glass sample corresponds to sample site "AO" in Tuffen and Castro (2009) and its bulk composition is reported by these authors (and repeated here in Table 1). We milled the glass in a (Retsch GmbH) centrifugal ball mill (S1000) under dry conditions (i.e., no acetone was used) at rates sufficiently slow to ensure no appreciable heating occurred, monitored qualitatively by stopping the mill periodically and checking for hot spots manually. The material was then sieved to obtain typical particle size distributions found in fall deposits for silicic eruptions (Zimanowski et al., 2003), denoted as, ≥90, 90-63 and <63 μm, that correspond to "very fine ash", "fine ash" and "medium ash", respectively (Rose and Durant 2009). The particle size distributions were obtained using a Beckman-

Coulter LS230 laser particle diffraction analyzer (full particle size distributions reported in Figure 1). The arithmetic means of the particle size distributions $\langle R \rangle$ are 22.6, 41.23 and 288 μm of <63, 63-90, and ≥90 μm, respectively. The specific surface area (in $m^2.g^{-1}$) of the starting material was determined using the Brunauer, Emmet and Teller (BET) method using a nine-point He-adsorption isotherm acquired with a Micromeritics Gemini III 2375 surface area analyser. The specific surface area measurements are given in Table 2. Approximate spot-analyses of particle glass chemistry and images of pre- and post-treated samples were determined using the back-scattered electron detector (BSED) on a Hitachi field-emission scanning electron microscope (FE-SEM) SU5000 equipped with energy dispersive spectrometers.

3.2 Experimental procedure

All ash-gas experiments were performed with the ash-gas reactor device described in Ayris et al., (2015) and illustrated in Figure 2. This is a customized apparatus that allows the experimental simulation of gas-ash or gas-magma reactions (Ayris et al. 2015) by mixing ash and gases in a rotating quartz bulb within a 3-zone furnace in which the temperature in the bulb and each of the zones was monitored using a K-type thermocouple accurate to within 2 ºC (Ayris et al., 2015). Two experimental conditions were used to treat the samples: (1) anhydrous, and (2) hydrous SO_2 atmospheres. The anhydrous condition consisted of a binary SO_2-Ar mixture, whereas the hydrous condition contained various additions of nebulized H_2O. The experiments were performed by exposing ~2 g of powdered glass from one of the particle size distributions to isothermal temperatures 200-800 °C for times from 1 to 60 minutes. The sample was placed inside the reactor bulb in a split 3-zone Carbolite HZS-12/-/900/E301 horizontal tube furnace. For the hydrous experiments, a SPETEC Perimax-12 low-flow peristaltic pump connected to a Meinhard Glass Products Q-HEN-150-A quartz nebulizer fed water into the system as an aerosol.

The gas mixture used for anhydrous conditions consisted in a 100 sccm gas stream consisting of 80 mol.% Ar and 1 mol.% SO_2 (Ar balance), plus a 225 sccm CP grade Ar flow as carrier gas. Calibration experiments at higher SO_2 mol.% did not alter the results.

To further test the behavior of monovalent cations (i.e., Na^+, K^+) diffusion under more oxidizing conditions, we also conducted an experiment with pre-oxidized material. This is relevant

because diffusion of monovalent cations strongly depends on their role in the melt (e.g., as charge compensating cations or network modifiers), which is in turn also influenced by the redox state of network former cations like iron. Consequently, we designed an experiment where the redox state of iron, expressed as $Fe^{3+}/\sum Fe_{tot}$, of the initial material was higher; 0.416 (thus, more oxidized), than its original value 0.153. This was achieved by pre-heating 2 g of original powdered glass, of the grain size distribution between 63 and 90 μm at 700 °C for one hour under an Ar-air atmosphere, to effectively relax the glass redox state. Following the pre-heating, the sample was treated under anhydrous conditions (SO_2-Ar) at 600°C for 1 h.

For the hydrous conditions, only the grain size distribution of 90-63 μm was used. This is justified because the underlying mechanisms of gas scavenging were elucidated in the anhydrous experiments, and the hydrous experiments are simply designed to test the difference that results from the addition of water. The temperature-series experiments were performed at 400-800 °C for 60 min. Eleven different flow rates of H_2O were used, ranging from 0.05 to 7 $ml.min^{-1}$ using the constant 1 mol.% SO_2 and 80 mol.% Ar. Under the conditions tested, this resulted in a mol.% proportion of H_2O of 0.01-96.41. In the case of H_2O vapour, these were selected by taking the flow rate range available of the peristatic pump used to nebulize water flow. At one flow rate of water (0.4 $ml.min^{-1}$) we conducted time-series experiments (1-60 minutes) at 600-800 ºC. We have chosen to neglect some of the high-flow rate data for which there was evidence that during cooling, condensation of water in the sample bulb caused washing of salt deposits prior to further analysis. We did not compute the change in gas composition due to mixing of the water and sulphur during the experiment.

We conducted an additional set of HCl, and HCl-H_2O experiments using the same material described above. Analogous to the SO2 anhydrous experiments, the HCl experiments were conducted in a 100 sccm gas stream of 80 mol% Ar and 1 mol.% HCl (Ar balance), an additional 225 sccm CP grade Ar stream was used as carrier gas.. For the anhydrous experiments, the HCl uptake of the material was tested for the three grain size distributions (<63, 63-90, >90μm); 2 gr of each grain size distribution were exposed to the HCl-Ar gas mixture for between 1 and 60 minutes, at between 200 and 800°C. For the hydrous experiments, additional to the above mentioned gas mixture, eleven water vapour flows

(0.05 to 7 ml.min^{-1}) were added. As in the case of the SO_2-H_2O experiments, only a single grain size was chosen to be tested at hydrous conditions (63-90), for 60 min at 400-800 °C.

Experiments were terminated by rapid quenching in air by removing the sample bulb quickly (up to 10 K.min^{-1}; Ayris et al., 2015). After each experiment, the samples were taken out of the reactor and left to cool to room temperature. The quenched samples were collected and stored in glass vials. We leached the samples at room temperature with deionized water (≤4.3 µS/cm) for 1 h at a 1:250 solid:water ratio, followed by filtration through 0.22 µm mixed cellulose ester membrane. Ion analyses were performed with a Metrohm ion chromatography system (733 separation center and 732 conductivity detector). Anions (Cl^-, SO_4^{2-}) and cations (K^+, Na^+, Ca^{2+} and Mg^{2+}) were analyzed with a Metrosep A Supp 5-150/4.0 and a Metrosep C4-150/4.0 column, respectively.

4. RESULTS

4.1 Scavenging in anhydrous sulphur atmospheres

SEM images of non-treated samples (not exposed yet to the high temperature gas mixture), showed nominally featureless glassy surfaces and a general blocky angular texture (Figure 3a). SEM-EDS analysis of samples of the three particle size distributions exposed to SO_2-Ar gas mixtures for 60 minutes at 800 ºC confirms that salt crystals of dominantly $CaSO_4$ composition (Figure 3b) and minor components of Na_2SO_4 are formed on ash surfaces.

Whereas SEM-EDS analyses confirm the approximate chemistry of the phases present, in order to gain quantitative insights into the kinetics of the sulphur scavenging process, we turn below to the time-series analysis of leachates.

Following exposure to SO_2-Ar gas mixtures at 200-800 ºC for 1-60 minutes, the most abundant leachable cation was Ca^{2+},amounting up to ~ 80% of the bulk Ca^{2+} content, followed by Na^+ (up to ~ 8%) and minor components of K^+ (up to ~ 0.6%) and Mg^{2+} (up to ~ 14%). The minor components K^+ and Mg^{2+} suggest that accessory potassium- and magnesium-bearing salts were formed on the surfaces, which were not directly identified in the SEM analysis. The glass leachate compositions in dry SO_2-Ar atmospheres are consistent with the broad conclusions obtained by Ayris et al. (2013) using SO_2-air atmospheres. (1) Total leached calcium increases with time non-linearly from low values at short

exposure times to values approaching 10^4 mg.kg^{-1} (Figure 4). (2) The time-dependence of the increase in leached Ca^{2+} is strongly dependent on particle size and exposure temperature. Large particles or low temperatures produce less Ca^{2+} for leaching than small particles or high temperatures (Figure 4a-c). (3) Total leached Na^+ or K^+ shows similar features to Ca^{2+}, however, there is a switch from a positive temperature-dependence of the leached amount of these cations Na^+ and K^+ to a negative dependence on temperature at >600 ºC (Figure 4d-i). This switch is similar in both Na^+ and K^+ data. At 800 ºC the concentrations are negligible for all times of exposure.

Concentrations of leached cations for the experiment performed with pre-heated (oxidized) material are presented in Table 3. In all cases the concentration of leached cations was lower for significantly lower for the experiments conducted with the pre-heated (i.e., pre-oxidized) powdered glass compared to those performed with the original powdered glass, with 68, 83 and 91 % less leached concentration of Ca, Na and K, respectively.

4.2 Adsorption and scavenging in hydrous sulphur atmospheres

After exposure to atmospheres of mixed SO_2 and H_2O, the experimental samples showed a diverse crystal assemblage that was absent on the pre-experimental sample surface and which differs from the experimentally produced surfaces in anhydrous conditions. SEM-EDS analysis confirmed the presence of calcium- and sulphur-bearing phases as the dominant components of the surface salts. Small 0.5-1 μm angular crystals broadly cover the surfaces (Figure 3b), while under hydrous conditions, the composition, morphology and distribution of the salts formed, appears to depend dominantly on the temperature and time of the experiments (Figs. 5a-b).

Figure 6 shows how the leachate concentrations for each given temperature vary as a function of mol.% H_2O. A horizontal line marks the anhydrous value of the leached element at the same temperature-time condition. We noted that the leached concentrations of Ca^{2+} are broadly consistent with the anhydrous values for the same temperature (Figure 6 a-e). In addition, leachate concentrations of both Na^+ and K^+ are significantly elevated relative to the anhydrous values for all temperatures <800 ºC. At 800 ºC the leachate concentrations are indistinguishable from those recorded in anhydrous conditions (Figure 6f-o).

To illustrate the differences between hydrous and anhydrous conditions, we examine explicitly in Fig. 7 the time-dependence of Na^+ and K^+ diffusion in both cases at fixed water concentration in the vapour phase (62.29 mol.% H_2O). Note that at 600 ºC the non-linear increase of concentration in the leachate analyses is amplified when H_2O vapour is present (Figure 7a and 7d). However, at 800 ºC there are negligible concentrations regardless of whether the atmosphere contained H_2O vapour (Figure 7c and 7f). Finally, at intermediate temperatures (700 ºC), the concentrations are negligible in anhydrous conditions (as noted in §3.2), but remain non-negligible in hydrous conditions and evolve in a qualitatively similar way to the corresponding time series of concentrations at 600 ºC (Figure 7b and 7e).

Analysis of the leachates from the samples treated with HCl and HCl-H_2O gas, the relevance of HCl scavenging by this material was found to be minor, in comparison of that of SO_2. This was also observed by Ayris et al. (2014), who also evaluated the HCl-scavenging potential of rhyolitic glass of similar composition to ours, and concluded no significant scavenging of HCl could be caused by this glass. In what follows, we concentrate on the SO_2 sequestration potential, and neglect HCl.

5. DISCUSSION

Our work provides a closer approximation of the processes developed in isolated (i.e., without air entrainment) ash-gas interaction at conduit to plume core conditions in large rhyolitic eruptions. For such eruptions, at short initial times after fragmentation, effectively no air can interact with either the ash or the gases at the plume inner core (Suzuki and Koyaguchi, 2012). Our results show that the extraction of cations from bulk particles is time, temperature and particle size dependent. Ayris et al. (2013) concluded that in anhydrous experiments Ca^{2+} moves toward the particle surface by diffusion. Diffusion is thereby limited by the value of the diffusivity D_x where x is replaced by the cation in question (e.g., D_{Ca} in the case of calcium diffusivity). Diffusivities of Ca, Na and K have been experimentally parameterized previously as a function of temperature (Zhang et al., 2010 and references therein), and have shown experimentally to be generally Arrhenius having the general form

$$D_x = D_0 \exp\left(-\frac{b}{T}\right) \quad \text{Eq. 1}$$

where D_o is the reference diffusivity ($m^2.s^{-1}$), b is an experimentally determined constant and T is the temperature, both b and T are expressed in Kelvin. We use published constraints of D_0 and b, in rhyolitic samples, listed in Table 4, to obtain temperature-dependent diffusion laws for $D_{\mathrm{Ca}}(T)$, $D_{\mathrm{Na}}(T)$, and $D_{\mathrm{K}}(T)$ which we can use to scale our experimental data for any temperature. For instance, the value of D_{Ca} for the anhydrous experiment (SO_2-Ar) at 800°C and at 60 min, was found to be $2.15 \times 10^{-17} \mathrm{m}^2.\mathrm{s}^{-1}$, which is similar to that obtained by Ayris et al., (2013), for rhyolitic glass powders at the same temperature and exposure time, e.g., $10^{-17} < D_{\mathrm{Ca}} < 10^{-18} \mathrm{m}^2.\mathrm{s}^{-1}$.

The characteristic timescale associated with diffusive mass transfer is $\lambda_D = R^2/D_x$ where, in the case of pseudo-spherical volcanic ash particles, R is the particle radius and particle angularity is neglected (Wadsworth et al., 2017a). Using $D_x(T)$ described above and using the arithmetic mean of the distribution of particle sizes $\langle R \rangle$ as a proxy for the characteristic length in polydisperse particle distributions (Wadsworth et al., 2017b), we can define λ_D for each suite of experiments at different temperatures, for each particle size distribution used, and for each cation of interest. If we assume that the total amount of each cation available for mass transfer is the initial total concentration of that oxide in the starting glass (Table 1), we can normalize the leachate concentrations C_x by their respective initial bulk values $C_{i,x}$ giving $\bar{C} = C_x/C_{i,x}$. And in each case, by normalizing the experimental time t by λ_D to give $\bar{t} = t/\lambda_D$, we demonstrate that the data follows a consistent trend of $\bar{C}(\bar{t})$ for most datasets (Figure 8).

Using the above scaling analysis we can clearly visualize the effects discussed in sections 3.1 and 3.2; namely, the apparent lack of Na and K diffusion above critical threshold temperatures (reflected in negligible concentrations in the leachate analyses; Figure 8b and 8c). For clarity, we cast the 700 and 800 ºC anhydrous time-series and the 800 ºC hydrous time-series data as unfilled data points in Figure 8. Using this distinction, it is clear to see that at these temperatures the diffusive extraction of Na^+ and K^+ to form surface salts is negligible compared with the consistent trend at lower temperatures. This is consistent with the observation that >600 ºC and >700 ºC are the threshold

temperatures in anhydrous and hydrous conditions, respectively. Here, we interpret these thresholds as representing a transition from reduced to oxidized above those threshold temperatures, and consequently as the switch from Fe^{2+} to Fe^{3+} (see Table 3), which has been shown to effectively capture Na^+ and K^+ for charge balancing (Cook and Cooper 2000; Cook et al., 1990; Cooper et al., 1996a,b, 1997).

In most cases, silicate liquid equilibrium oxygen fugacity will increase with increasing temperature, implying more oxidising conditions at higher relative temperatures (e.g. Sack et al., 1980). On reheating in our experimental apparatus, the glass will relax above the glass transition temperature (approximately 700 °C using a viscosity threshold of 10^{12} Pa.s as an approximation of the glass transition, and using the model of Hess & Dingwell (1996) with a dissolved water content of 0.18 wt.%). Relaxation of silicate structure in our experiments will allow equilibration of the redox state, which in turn may be more oxidizing than the conditions locked in during cooling in nature (see Dingwell, 1990 for a review). Outstanding questions surround the effect of the total amount of available Fe, or of bulk composition, on the transition temperature. In order to further test that oxidation of Fe^{2+} to Fe^{3+} occurring at T> 600 °C, induces a reduction of Na^+ and K^+ diffusion amplitude, we pre-heated 2g of our sample material at 700 °C for one hour to effectively relax the structure and redox state in the glass network, and then treated at 600 °C under anhydrous conditions (SO_2-Ar) for 1h. The leaching results show significantly less leached Na^+ and K^+ compared with the sample that was not relaxed at high temperature first (Table 3; Supplementary Material).

Although the data for $\bar{C}(\bar{t})$ fall to a universal trend in Fig. 8, in both the hydrous and anhydrous regimes, the data collected in hydrous atmospheres are at higher $\bar{C}$ for any given $\bar{t}$, consistent with the observations in dimensional plots (Figure 7). Therefore, it is likely that a non-negligible effect of H_2O on the diffusive process. Koenderink et al. (2000) showed that diffusion of H^+ (or H_3O^+) in sodium silicate glasses containing Mg^{2+}, Ca^{2+}, $Sr^{2+}$and Ba^{2+}, can exchange with equi-valent Na^+ or K^+ generating ion exchange. Our inferred increase of the diffusive potential in the presence of H_2O vapour can therefore be interpreted as the effect of inward migration of H^+ enhancing the outward migration of Na^+ and K^+ up until the threshold temperature for surface oxidation described above. Indeed, the fact that the threshold temperature for oxidative cut-off of diffusion of Na^+ and K^+ is dependent on H_2O (Figure 6) suggests that these effects of oxidation and ion exchange by motion of H^+ compete with one

another. The implication is that this oxidation threshold is apparently higher in hydrous conditions at low H_2O activity when H^+ ion exchange dominates over oxidation (Figure 6-8) but is independent of humidity at high H_2O when oxidation dominates over H^+ ion exchange (Figure 6).

6. HIGH-TEMPERATURE SCAVENGING IN DOME FRACTURES: A CASE STUDY OF VOLCÁN CHAITÉN 2008

We now apply our findings to an in-dome scenario, a system that can be open, fractured and permeable to magmatic gas flow. Fractures in lava domes frequently host veins filled with fine-grained volcanic ash and host-rock material (i.e. tuffisites) and reflect processes occurring within the volcanic conduit (Tuffen at al., 2003; Kolzenburg et al., 2012).

Taking the case of the lava dome erupted at Volcán Chaitén (Chile) in May 2008, we can scale for the amount of SO_2 sequestered in reasonable time limits. Our study has found that the important parameters are temperature T, which conveys a diffusivity D_x, the timescale available at high temperature for sequestration t, particle size(s), captured by the arithmetic mean $\langle R \rangle$, and the initial amount of the cation in question C_i. For the reactions involving Na^+ and K^+, we additionally show that the presence of H_2O in the gas phase is an additional key parameter.

In-conduit or in-dome conditions are inevitably hot for longer than a rapidly ascending plume. Fracture networks are pervasive at silicic conduit margins (Farquharson et al., 2017; Gonnermann and Manga, 2003, Tuffen and Castro 2009) and are advected up into domes, providing open-system pathways for gas transport bypassing melt. Such systems are typically in chemical disequilibrium at fracture and particle surfaces, especially while cooling, and gas-melt back-reactions can be common (e.g., Berlo et al., 2013; Schipper et al., 2015). Here we explore the possibility of back-reactions occurring during SO_2-rich gas transport through tuffisite veins in the dome of Volcán Chaitén soon after emplacement in May 2008 (Castro et al., 2012). Such a tuffisite vein is shown in Figure 9 collected as part of a larger bomb (analysis of this bomb appears in Saubin et al., 2015).

Castro and Dingwell (2009) and Castro et al. (2012) provide a storage and ascent temperature estimate of $T = 825$ ºC. Castro et al. (2012) additionally explore fracture dynamics at $T = 625$ ºC, an

estimated calorimetric glass transition temperature (Giordano et al. 2008). Both 825 and 625°C represent the temperatures at which diffusion would have taken place within the tuffisites. We then use the constraints presented previously to find that $D_{\mathrm{Ca}} = 4 \times 10^{-17}$ m^2.s^{-1}, $D_{\mathrm{Na}} = 1.2 \times 10^{-10}$ m^2.s^{-1}, and $D_{\mathrm{K}} = 3.1 \times 10^{-12}$ m^2.s^{-1} for 825 ºC, and $D_{\mathrm{Ca}} = 9.6 \times 10^{-20}$ m^2.s^{-1}, $D_{\mathrm{Na}} = 1.6 \times 10^{-11}$ m^2.s^{-1}, and $D_{\mathrm{K}} = 2.3 \times 10^{-13}$ m^2.s^{-1} for 625 ºC. Such rhyolitic lava domes are frequently fractured and the fractures often host partially welded, initially granular tuffisites (e.g., Tuffen and Dingwell, 2005). At Volcán Chaitén, the grain sizes in these tuffisites range approximately from 0.1 to 1 mm (see dense clasts in a "main vein" measured in Saubin et al., 2015). This permits us to convert D_x to λ_D for each cation, and so, taking maxima and minima conditions (from maximum and minimum $\langle R \rangle$), and taking $T = 825$ ºC, we find that $10^8 < \lambda_D < 10^{10}$ s for Ca diffusion, $10^1 < \lambda_D < 10^3$ s for Na diffusion and $10^3 < \lambda_D < 10^5$ s for K diffusion. For $T = 625$ ºC, these timescales would be $10^{11} < \lambda_D < 10^{13}$, $10^2 < \lambda_D < 10^4$, and $10^4 < \lambda_D < 10^6$ s, respectively.

A first-order timescale for the time available for the diffusion-limited SO_2 sequestration process to occur is the timescale that these welding fractures can stay open and permeable (Wadsworth et al., 2014). This is approximated by the sintering timescale λ_s for particles sintering at high temperatures, and is $\lambda_s = \mu\langle R \rangle/\Gamma$, where μ is the viscosity, and $\Gamma \approx 0.3$ N.m^{-1} is the surface tension with the gas phase (Wadsworth et al., 2016). In detail, Γ depends on the gas species available, but the value quoted here is an approximate and within the correct order of magnitude (Parikh, 1958). Given the range of water contents 0.2-0.95 wt.% in the dome glasses (Castro et al., 2012), we can use the viscosity model from Hess and Dingwell, (1996) for rhyolites to find that μ is of the order $10^7 - 10^9$ Pa.s at this temperature. We then find that $10^3 < \lambda_s < 10^{10}$ s. If we take $\lambda_s \sim t$, this gives us t/λ_D ranges of $10^{-7} - 10^{-2}$ for Ca^{2+}, $10^{-1} - 10^4$ for Na^+, and $10^{-2} - 10^3$ for K^+ at $T = 825$ ºC. Referring to Figure 8, these t/λ_D ranges would be sufficient for ~30-90% of the initial Ca^{2+} in the welding particles to be available for surface reactions with SO_2. Similarly, ~0-20% Na^+ and negligible amounts of K^+ would contribute in anhydrous conditions. In hydrous conditions, we can read from Figure 8 that this would increase to ~0-50% of the initial Na^+ and <5% of K^+. Interestingly, at the lower example temperature $T = 625$ ºC, while the values of λ_D are increased relative to the higher temperature (see above), the overall value of t/λ_D is increased because λ_s is much longer. This is of interest as it shows that across

these range of conditions, the time for which the dome fractures can remain open exerts a controlling role during cooling compared with the time required for diffusion.

Next, we have to scale the above constraints to the dome scale. Gonnermann and Manga (2003) compute a fractured zone at the margins of rhyolitic conduits of radius L that has thickness δ such that $\delta = FL\mu^{0.1}$ where $F = 0.01$ Pa.s$^{-0.1}$ is the given proportionality. Castro et al. (2012) constrain L to be 50 m on the basis of aerial views of the dome during the initial eruption and μ is given above. We therefore find that δ is between 2.6 and 9.7 m for the range of parameters given above. Within the fracture zone δ we can assume we have n fractures with thickness l_f and inter-fracture spacing l_s such that $\delta = n(l_f + l_s)$. In cylindrical coordinates, we can compute the cross sectional area of fractures that occupy the damage zone δ, which we term A_f. A_T is then the total area $A_T = \pi L^2$. A_f then relates to l_f and l_s via

$$A_f = \sum_{j=1}^{n} A_{f,j} \qquad \text{Eq. 2}$$

and the *jth* fracture has area $A_{f,j} = \pi\left[(2j-1)l_f^2 + 2l_f(L - \delta + l_s)\right]$. Converting A_f to the cumulative mass of glass particles m_g in the fractures will be necessary to compute mass fractions of SO_2 scavenged and can be achieved by

$$m_g = A_f H \rho (1 - \phi_i) \qquad \text{Eq. 3}$$

where H is the vertical depth to which the fractures penetrate in the conduit, ρ is the glass density and ϕ_i is the initial porosity in each fracture. Wadsworth et al. (2016; 2014) found that an approximate value of $\phi_i = 0.5$ valid for most realistic packs of particles is of relevance to tuffisite emplacement.

Knowing the mass of each cation in the glass that is available for reaction with the gas phase in the time available, m_x, by $m_x = C_x C_{i,x} m_g$, (and the reaction given in section 2) we can find the mass of SO_2 that will react with a given m_x by $m_{SO_2} = M_{SO_2} m_x / M_x$, where M_{SO_2} is the molar mass of SO_2 and M_x is the molar mass of the reacting cation species. Now the mass fraction of the total exsolved SO_2 that

can be scavenged is $S = m_{SO_2}/(m_{SO_2} + m_e)$ where m_e is the total mass of exsolved SO_2 in the gas phase. As a limiting assumption, we simply take the value of the 500 mg.kg^{-1} SO_2 (which we term C_{i,SO_2}) as the initial available proportion of the total mass that is released at the surface, measured in glass inclusions from the Plinian pumice eruption in May 2008 (Castro et al., 2012). This amount can be converted to m_e by

$$m_e = \phi_i A_T H \rho C_{i,SO_2} \qquad \text{Eq. 4}$$

This assumption requires that all the SO_2 that is exsolved into the gas phase originates from the same volume $A_T H$ in which the fractures occur. This simplifying assumption means the sequestration efficiency S is independent of the H over which the fractures occur.

The initial amount of Ca, Na, and K in the glass phase can be estimated using the rapidly ejected pumice analysed in Castro and Dingwell (2009) as $C_{i,x}$ of 0.014, 0.04 and 0.03 mass fraction, respectively (note that in Castro and Dingwell, 2009, these values appear as wt.%). With these values and the inputs given above, we find that the value of S that is attributable to calcium's role in the sequestration is 0.12-0.5. The amount attributable to Na is up to 0.4 in hydrous conditions. Summing these contributions we predict that between 12 and 90% of the eruptible sulphur dioxide can be scavenged during permeable flow through welding fractures (with 12% referring to the limiting 625 ºC and 90% referring to the eruptive 825 ºC, considered here).

These estimates are maxima if we acknowledge that the total erupted SO_2 may not be from the volume $A_T H$, and may only be from $A_f H$. Furthermore, these constraints would be overestimates if we consider that additional SO_2 may be bypassing the transiently open tuffisites from depths greater than H. Nonetheless, the results are striking that in-dome scavenging may be efficient over the timescales of open-system outgassing. Additional complexities may arise from the complex geomertries of many particles entrained and welded in tuffisite outgassing channels (e.g. Castro et al., 2012; Saubin et al., 2015).

The result found above suggests that rhyolitic volcanic domes that are heavily fractured and for which the fractures are the dominant outgassing pathway (e.g., Castro et al., 2012; Tuffen et al., 2003;

Cabrera et al., 2008), may act as efficient filters for the bulk SO_2 emitted. For the case of Volcán Chaitén (2008 eruption), this is broadly consistent with the "remarkably low" SO_2 measured in the plume above the emerging dome (Carn et al. 2009). Whereas no concrete evidence (i.e., $CaSO_4$, Na_2SO_4, etc. growth in tuffisite samples) for the Chaitén dome have been found, this could be attributed to dissolution upon contact with meteoric water.

7. CONCLUSIONS

We have confirmed that high-temperature scavenging of SO_2 is a plausible mechanism to remove sulphur from volcanic glassy ash. We use scaled experiments to parameterize the problem and find that SO_2 scavenging is diffusion-limited at high temperatures. We demonstrate that this can be scaled using published Ca^{2+} diffusivity values, implying that Ca^{2+} diffusion from the ash bulk toward the surface is the limiting factor in the formation of $CaSO_4$ salt deposition, which in turn acts as the sink for the SO_2. We identify that the dominant effect of humidity (H_2O) is in limiting the diffusion of Na^+ and K^+ to the ash surface and explain this in terms of an oxidation reaction. However, we find that humidity is not limiting in Ca^{2+} diffusion, which occurs irrespective of the partial pressure of water. We apply these observations to a case study of the 2008 eruption at Volcán Chaitén for which we show that in-dome fractures may efficiently scavenge large proportions of the eruptible SO_2. These simple calculations lead us to suggest that rhyolitic domes may scrub volcanic gases of sulphur and reduce the amount available for atmospheric interactions.

Acknowledgements

A.S.C. was funded by a CONACyT-DAAD PhD scholarship (Nr. 409903). Additional funding was provided by AXA Research Grant "Risk from volcanic ash in the Earth system" to D.B.D. The tuffisite vein in Figure 9 was collected by F.B.W. along with Hugh Tuffen, Ian Schipper and Jonathan Castro, all of whom are thanked heartily as well as fieldwork discussion with Kim Berlo, Amy Chadderton and Peter Sammonds. We are indebted to David Damby for informative discussion.

References

Ayris, P.M., Cimarelli, C., Delmelle, P., Wadsworth, F.B., and Vasseur, J. (2015). SHORT SCIENTIFIC COMMUNICATION. A novel apparatus for the simulation of eruptive gas-rock interactions. http://doi.org/10.1007/s00445-015-0990-3.

Ayris, P. M., and Delmelle, P. (2012). The immediate environmental effects of tephra emission. Bulletin of Volcanology, 74(9), 1905–1936. http://doi.org/10.1007/s00445-012-0654-5.

Ayris, P. M., Delmelle, P., Cimarelli, C., Maters, E. C., Suzuki, Y. J., and Dingwell, D. B. (2014). HCl uptake by volcanic ash in the high temperature eruption plume : Mechanistic insights. Geochimica et Cosmochimica Acta, 144, 188–201. http://doi.org/10.1016/j.gca.2014.08.028.

Ayris, P.M., Lee, A.F., Wilson, K., Kueppers, U., Dingwell, D.B., and Delmelle, P. (2013). SO 2 sequestration in large volcanic eruptions : High-temperature scavenging by tephra. Geochimica et Cosmochimica Acta, 110, 58–69. http://doi.org/10.1016/j.gca.2013.02.018.

Cabrera, A., Weinberg, R.F., Wright, H.M.N., Zlotnik, S., Cas, R.A.F. (2011). Melt fracturing and healing: a mechanism for degassing and origin of silicic obsidian. Geology 39, 67–70.

Carn, S.A., Clarisse, L., Prata, A.J. (2016). Multi-decadal satellite measurements of global volcanic degassing. J. Volcanol. Geotherm. Res. 311, 99-134.

Castro, J.M., Dingwell, D.B. (2009). Rapid ascent of rhyolite magma at Chaitén volcano, Chile. Nature, 461.(doi:10.1038).

Castro, J. M., Cordonnier, B., Tuffen, H., Tobin, M. J., Puskar, L., Martin, M. C., and Bechtel, H.A. (2012). The role of melt-fracture degassing in defusing explosive rhyolite eruptions at volcán Chaitén, Earth Planet. Sci. Lett., 333–334, 63–69.

Cook, G.B., and Cooper, R.F. (2000) Iron concentration and the physical processes of dynamic oxidation in an alkaline earth aluminosilicate glass. Am. Mineral. 85, 397–406.

Cook, G.B., Cooper, R.F., and Wu, T. (1990) Chemical diffusion and crystalline nucleation during oxidation of ferrous iron–bearing magnesium aluminosilicate glass. Journal of Non-Crystalline Solids, 120, 207–222.

Cooper, R.F., Fanselow, J.B., and Poker, D.B. (1996a) The mechanism of oxidation of a natural basaltic glass: Chemical diffusion of network-modifying cations. Geochimica et Cosmochimica Acta, 60, 3253–3265.

Cooper, R.F., Fanselow, J.B., Weber, J.K.R, Merkley, D.R., and Poker, D.B. (1996b). Dynamics of oxidation of a basaltic melt. Science, 274, 1173–1176.

Cooper, R.F., Smith, D.R., and Cook, G.B. (1997) Dynamic oxidation and the structure and crystallization of aluminosilicate glasses and melts. Electrochemical Society Proceedings, 97–39, 389–396.

Delmelle, P., Lambert, M., Dufrêne, Y., Gerin, P., and Óskarsson, N. (2007). Gas / aerosol – ash interaction in volcanic plumes : New insights from surface analyses of fine ash particles, 259, 159–170. http://doi.org/10.1016/j.epsl.2007.04.052.

Dingwell, D.B. (1990) Effects of structural relaxation on cationic tracer diffusion in silicate melts. Chemical Geology 82, 209-216.

Farquharson, J.I., Baud, P., Heap, M.J. (2017). Inelastic compactation and permeability evolution in volcanic rock. Solid Earth, 8, 561-581. https://doi.org/10.5194/se-8-561-2017.

Giggenbach, W.F. (1996). Chemical composition of volcanic gases, In: R. Scarpa and R. Tilling (eds), Monitoring and Mitigation of Volcano Hazards, Springer-Verlag, Berlin, 221-256.

Gonnermann, H.M., Manga, M. (2003). Explosive volcanism may not be an inevitable

consequence of magma fragmentation. Nature 426, 432–435.

Hess, K.U., Dingwell, D.B. (1996). Viscosities of hydrous leucogranitic melts: A non-Arrhenian model. Am. Mineral. 81, 1297–1300.

Jambon, A. (1982). Tracer diffusion in granitic melts: Experimental results for Na, K, Rb, Cs, Ca, Sr, Ba, Ce, Eu to 1300 °C and a model of calculation. J. Geophys. Res. 87, (10) 10797-10810.

Koenderink, G.H., Brzesowsky, R.H., and Balkenende, A.R. (2000). Effect of the initial stages of leaching on the surface of alkaline earth sodium silicate glasses. J. Non-Cryst. Solids 262 (1), 80-98.

Kolzenburg, S., Heap, M.J., Lavallée, Y., Russell, J.K., Meredith, P.G., and Dingwell, D.B. (2012). Strength and permeability recovery of tuffisite-bearing andesite. Solid Earth, 3, 191-198. https://doi.org/10.5194/se-3-191-2012.

Magaritz, M., and Hofmann, A.W. (1978). Diffusion of Sr, Ba and Na in obsidian. Geochim. Cosmochim. Acta 42, 595-605.

Maters, E.C., Delmelle, P., Rossi, M.J., Ayris, P.M. (2017). Reactive uptake of sulfur dioxide and ozone on volcanic glass and ash at ambient temperature. Journal of Geophysical Research: Atmospheres, 122. https://doi.org/10.1002/2017JD026993.

Mungall, J.E., Dingwell, D.B., Chaussidon, M. (1999). Chemical diffusivities of 18 trace elements in granitoid melts. Geochim. Cosmochim. Acta, 53, vol. 17, 2599-2610.

Mungall, J.E. (2002). Roasting the mantle: Slab melting and the genesis of major Au and Au-rich Cu deposits. *Geology* ; 30 (10): 915–918. doi: https://doi.org/10.1130/00917613(2002)030<0915:RTMSMA>2.0.CO;2

Óskarsson, N. (1980). The interaction between volcanic gases and soild tephra. J. Volcanol. Geotherm. Res., 8, 251–266.

Rose, W.I. (1977). Scavenging of volcanic aerosol by ash : Atmospheric and volcanologic implications. Geology, 5, 621–625.

Rose W.I., Durant, A.J. (2009). Fine ash content of explosive eruptions. J. Volcanol. Geotherm. Res. 186(1–2):32–39

Sack, R.O., Carmichael, I.S.E, Rivers, M.L., Ghiorso, M.S. (1980). Ferric-ferrous equilibria in natural silicate liquids at 1 bar. Contrib Mineral Petrol 75: 369–376.

Saubin, E., Tuffen, H., Gurioli, L., Owen, J., Castro, J.M., Berlo, K., McGowan, E.M., Schipper, C.I., Wehbe, K. (2016). Conduit dynamics in transitional rhyolitic activity recorded by tuffisite vein textures from the 2008–2009 Chaitén eruption. Front. Earth Sci. 4, 59.

Schipper, C.I., Castro, J.M., Tuffen, H., Wadsworth, F.B., Chappell, D., Pantoja, A.E., Simpson, M.P., Le Ru, E.C. (2015). Cristobalite in the 2011-2012 Cordón Caulle eruption (Chile). Bull. Volcanol., 77:34. https://doi.org/10.1007/s00445-015-0925-z.

Suzuki, Y.J. and Koyaguchi, T. (2012). 3-D numerical simulations of eruption column collapse: effects of vent size on pressure-balanced jet/plumes. J. Volcanol. Geoth. Res. 221, 1-13.

Symonds, R.B., Rose, W.I., Bluth, G.J.S., Gerlach, T.M., (1994). Volcanic gas studies: methods, results and applications. In: Carroll, M.R., Hollaway, J.R. (Eds.), Volatiles in

Magmas, Rev. Mineral., vol. 30. Mineralogical Society of America, pp. 1–66.

Textor, C., Graf, H.F., Timmreck, C., Robock, A. (2004). Emissions from volcanoes. In: Granier, C., Reeves, C., Artaxo, P. (Eds.), Emissions of Chemical Compounds and Aerosols in the Atmosphere, Advances in Global Change Research Vol. 18. Kluwer, Dordrecht, pp. 269 – 303.

Tuffen, H., Dingwell, D.B., Pinkerton, H. (2003). Repeated fracture and healing of silicic magma generate flow banding and earthquakes? Geology 31:1089–1092.

Tuffen, H., and Dingwell, D. (2005). Fault textures in volcanic conduits: Evidence for seismic trigger mechanisms during silicic eruptions. Bulletin of Volcanology, v. 67, p. 370–387, doi:10.1007/s00445-004-0383-5.

Tuffen, H., & Castro, J.M. (2009). The emplacement of an obsidian dyke through thin ice: Hrafntinnuhryggur, Krafla Iceland. J. Volcanol. Geotherm. Res., 185(4), 352–366. http://doi.org/10.1016/j.jvolgeores.2008.10.021.

Wadsworth, F.B., Vasseur, J., Von Aulock, F.W., Hess, K.U., Scheu, B., Lavallée, Y. and Dingwell, D.B. (2014). Nonisothermal viscous sintering of volcanic ash. J. Geophys. Res. Solid Earth, 119, 8792-8804, doi: 10.1002/2014JB011453.

Wadsworth, F.B., Vasseur, J., Llewellin, E.W., Schauroth, J., Dobson, K.J., Scheu, B. and Dingwell, D.B. (2016). Sintering of viscous droplets under surface tension. Porc. R. Soc. A. .DOI: 10.1098/rspa.2015.0780.

Wadsworth, F.B., Vasseur, J., Llewellin, E.W., Genareau, K., Cimarelli, C., Dingwell, D.B., (2017a). Size limits for rounding of volcanic ash particles heted by lightning. J. Geophys. Res. Solid Earth, 122, doi:10.1002/2016JB013864.

Wadsworth, F.B., Vasseur, J., Llewellin, E.W., Cimarelli, C., Dingwell, D.B. (2017b). Sintering of polydisperse viscous droplets. Physical Review E 95, 033114. doi: 10.1103/PhysRevE.95.033114.

Watson, E.B. (1981). Diffusion in magmas at depth in the earth: The effects of pressure and dissolved H2O. Earth Planet. Sci. Lett. 52, 291-301.

Wieczorek-Ciurowa, K. (1992) The thermal behaviour of compounds in the Ca–S–O system. J. Therm. Anal. 38, 523–530.

Zhang, Y., Ni, H., Chen, Y. (2010).Diffusion Data in Silicate Melts. Reviews in Mineralogy & Geochemistry. 72, 311-408.

Zimanowski, B., Wohletz, K., Dellino P., Büttner, R. (2003) The volcanic ash problem. J. Volcanol. Geotherm. Res. 122(1–2):1–5

Figure 1. Particle size distributions of the three sieved populations of rhyolitic ash grains. In shades of green, orange and blue are, respectively, the size distribution ranges <63 μm, 63-90 μm, and >90 μm, referred to in the text. We note that indeed, there are particles with radii <63 m in the 63-90 m and so these names are simply descriptive of which distribution is used, rather than quantitative. Shown here are 8 measurements with each powder.

Figure 2. (a) Schematic of the experimental apparatus described in detail in Ayris et al. (2015). The apparatus consists of a split 3-heating element tube furnace with a reactor tube inserted into it. At the end of the reactor tube is a bulbous sample holding head which is open at both ends to allow the flux of gas. The whole reactor tube rotates, tumbling particulate samples. Through the furnace assembly, SO_2-Ar gas mixtures, and nebulized H_2O droplets are flushed at known concentrations. (b) A schematic approximation of the process examined in this study showing a spherical rhyolitic particle with radius R (radial position r) that has developed a strong concentration gradient of calcium as $CaSO_4$ crystals grow on the surface.

Figure 3. Scanning electron microscope images of the typical crushed obsidian particles used in this study (a) prior to exposure to gas mixtures at high temperature, and (b) after exposure to SO_2-Ar at 800 C for 60 minutes. *Inset*: EDS spectrum of the species of interest S, K, and Ca. Absence of the sulphur peak in (a) the pristine samples suggests sulphur-bearing salt growth occurs due to treatment. Similarly, an increase in the calcium at the post-treated sample spectrum (b), with respect to that of pristine samples (a), suggests higher concentration due calcium diffusion.

Figure 4. Raw time-series data for (a-c) Ca^{2+}, (d-f) Na^+, and (g-i), K^+ cation concentrations for a range of temperatures of exposure and for (a), (d) and (g) <63 μm, and for (b), (e) and (h) 63-90 μm, and for (c), (f) and (i) >90 μm, where the labels in panel (c) correspond to values in ºC. We note that for any given time while high temperatures result in higher values of Ca^{2+}, this is not true above ~600 ºC for Na^+, or K^+, which is discussed in the main text.

Figure 5. SEM images of post-experimental sample surfaces after exposure to SO_2-H_2O-Ar at the values of P_{H_2O} labelled at 600 ºC for 60 minutes.

Figure 6. The effect of water flow rate, converted to partial pressure of water vapour P_{H_2O}, on scavenging processes for (a-e) calcium concentrations, (f-j) sodium concentrations, and (k-o) potassium concentrations. Horizontal lines are the measured value in anhydrous conditions at the same temperature. All samples are the 63-90 μm particle size distribution (Figure 2) and the exposure time was 60 minutes in each case.

Figure 7. Direct comparison of the time-dependence of surface concentration in hydrous (63.12 kPa) and anhydrous conditions at 600, 700 and 800 C for the 63-90 μm particle size distribution for (a-c) sodium and (d-f) potassium. We note that calcium does not display significant differences between hydrous and anhydrous conditions (Figure 6).

Figure 8. The concentration of a given cation$C_x(t)$, i.e., C_{Ca}, C_{Na}, C_K, (a, b and c, respectively) normalized by the initial value of that oxide C_i giving $\bar{C} = C_x/C_i$, as a function of time t normalized by the diffusion time λ_D, giving $\bar{t} = t/\lambda_D$. Using $\lambda_D = \langle R \rangle^2/D_x$ collapses the data over all temperatures and particle size distributions below the critical oxidation temperatures (above which diffusive mass transport to the surface is negligible). Vertical dashed lines simple guide the eye to a normalized time of unity.

Figure 9. A photograph of a fracture in rhyolitic obsidian from Volcán Chaitén. This sample is from a larger bomb erupted from the 2008 dome. The fracture is filled with a polydisperse distribution of volcanic ash and glass fragments. This geometry is the basis for our calculated sequestration efficiencies.

Figure 1

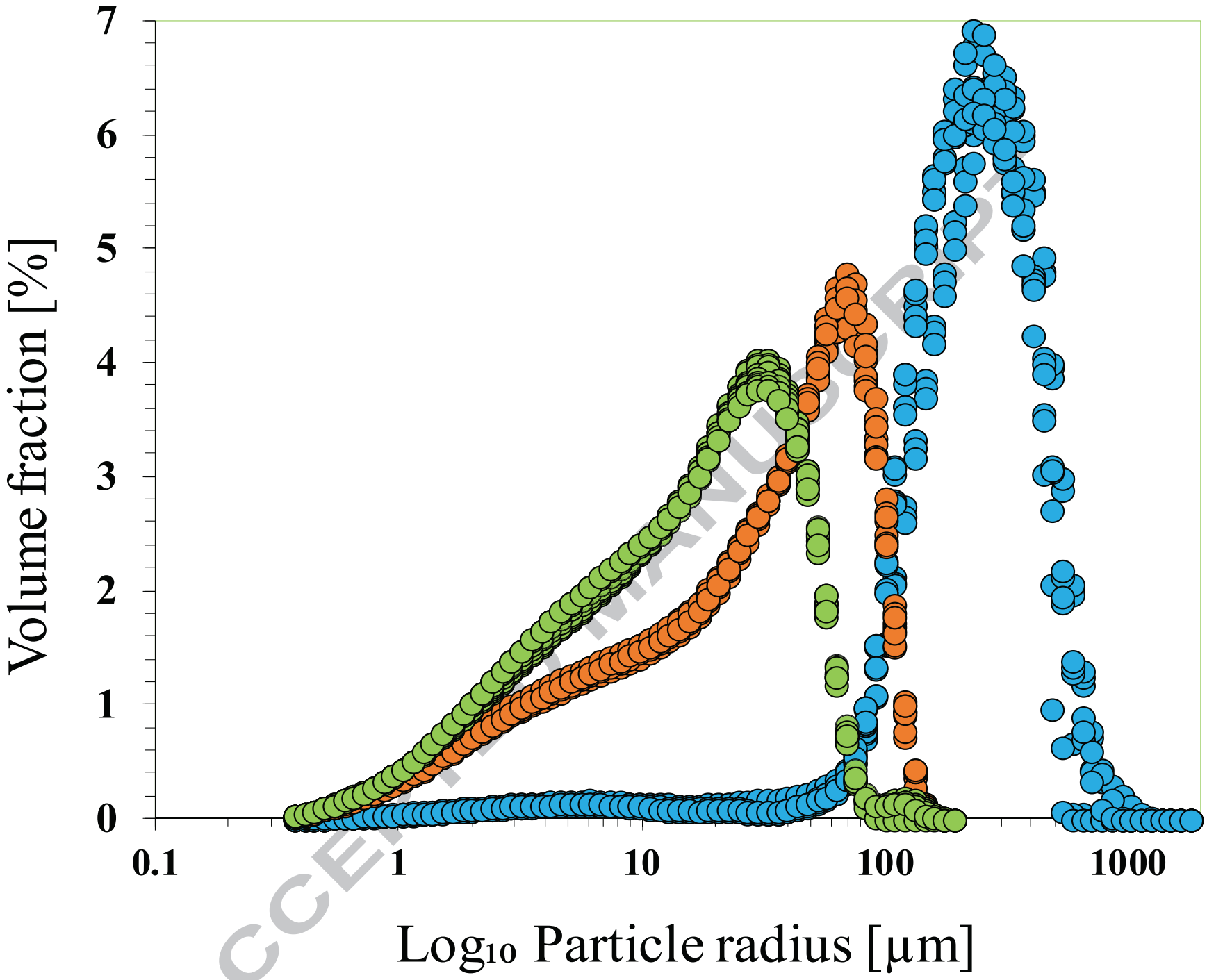

Figure 2

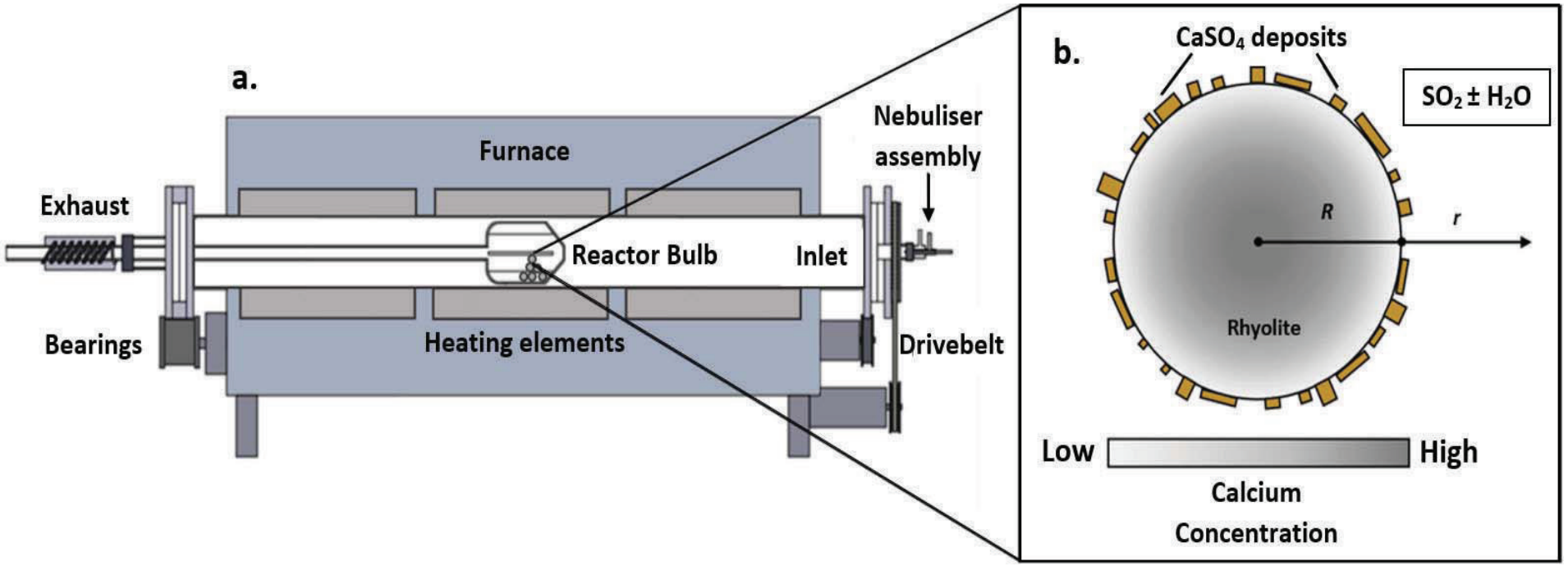

Figure 3

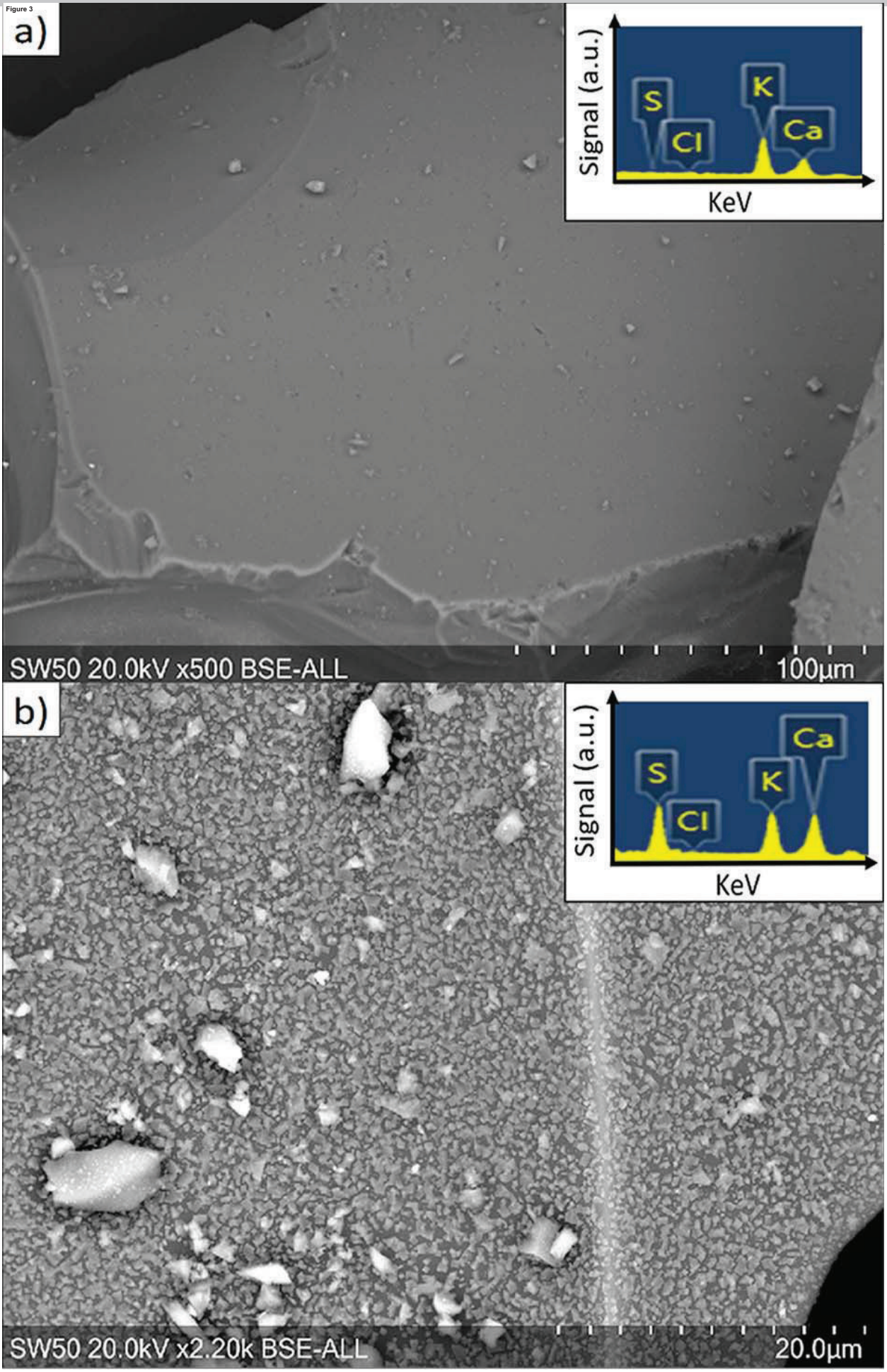

Figure 4

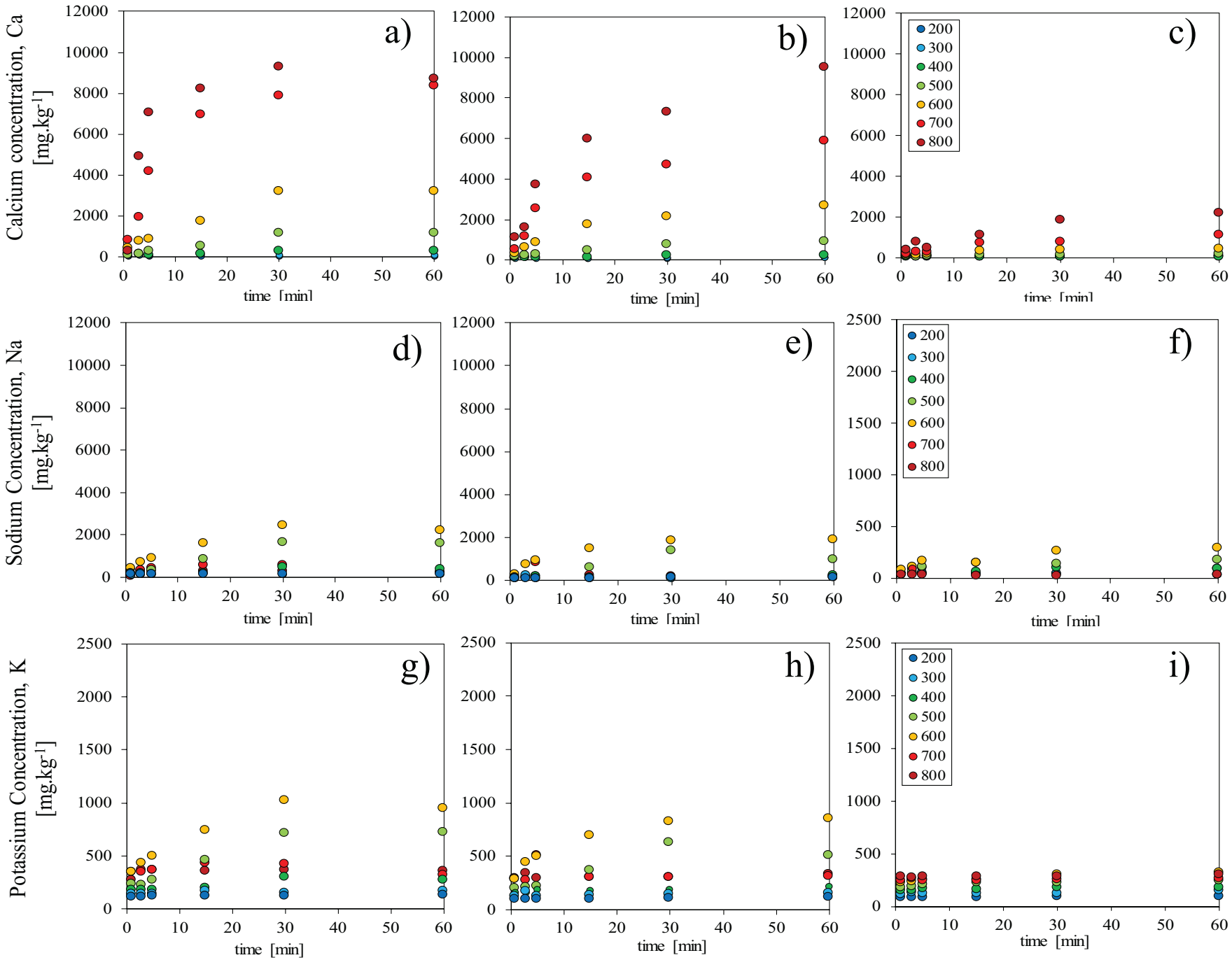

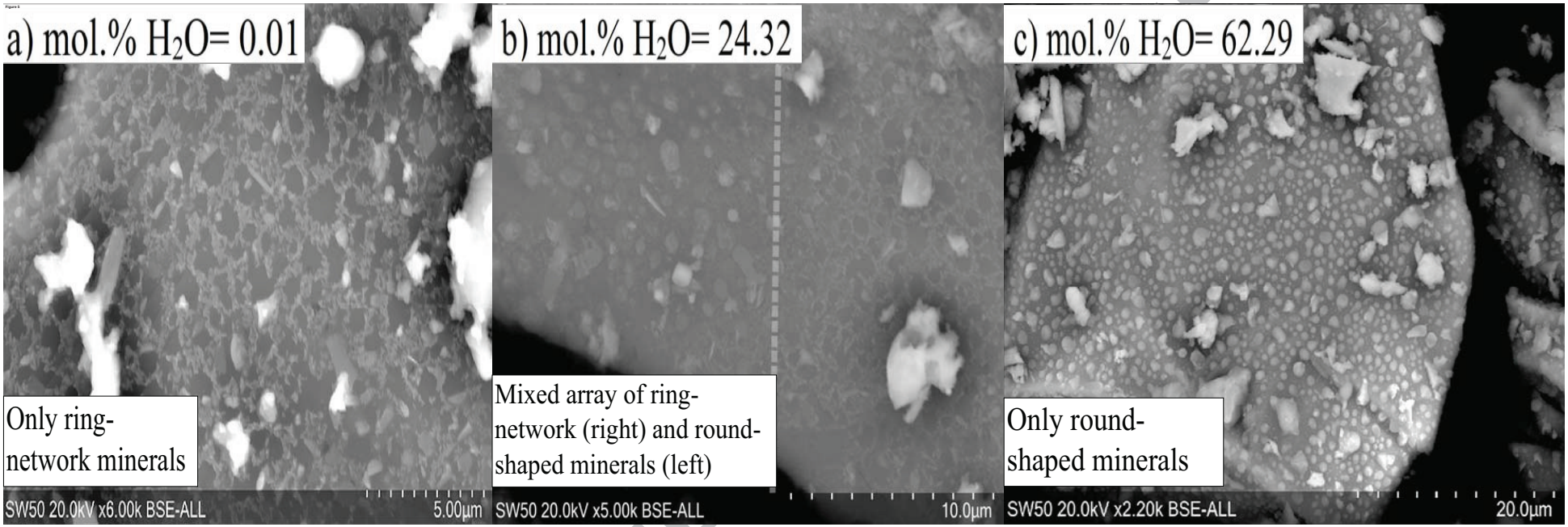

Figure 6

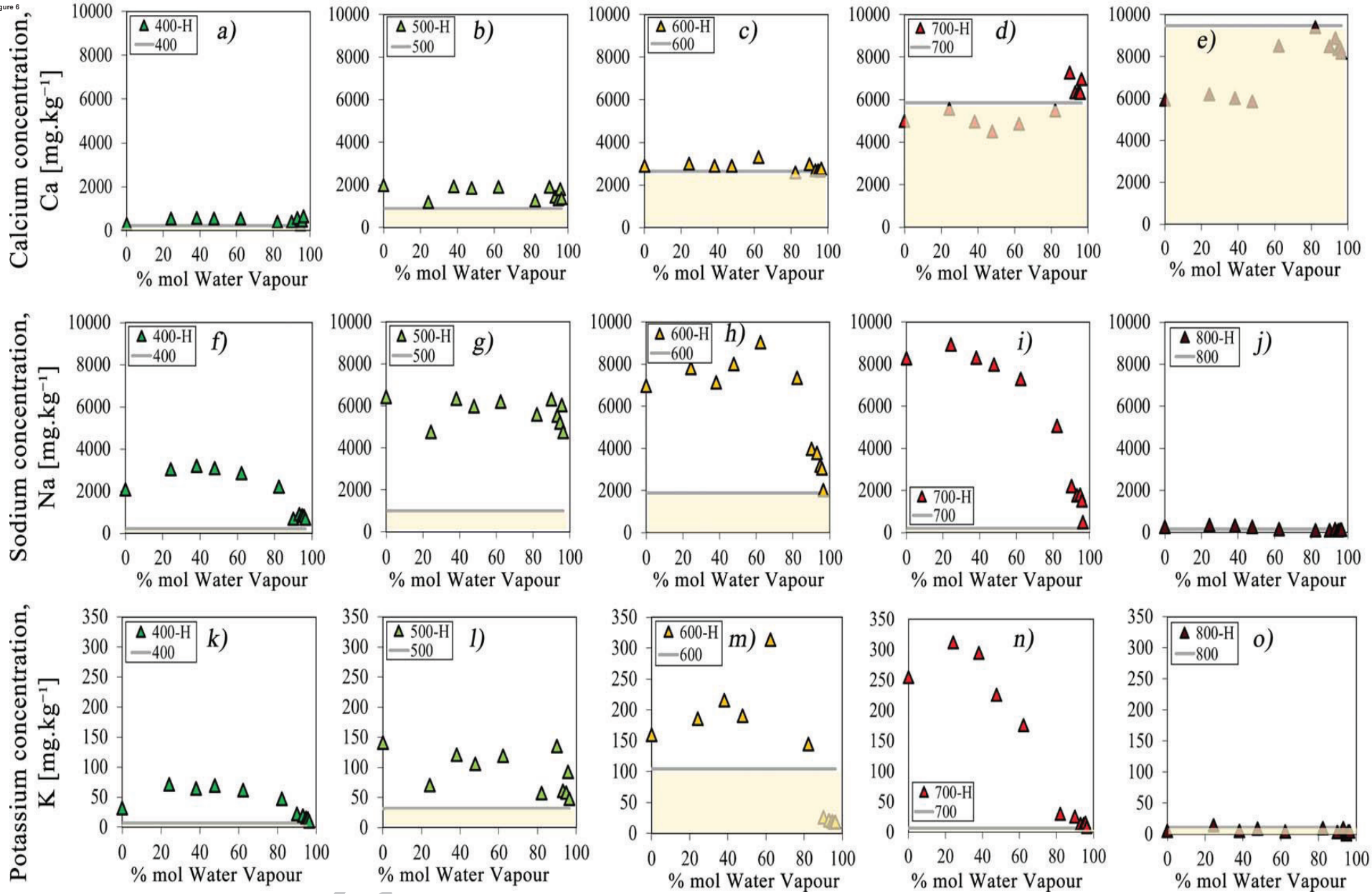

Figure 7

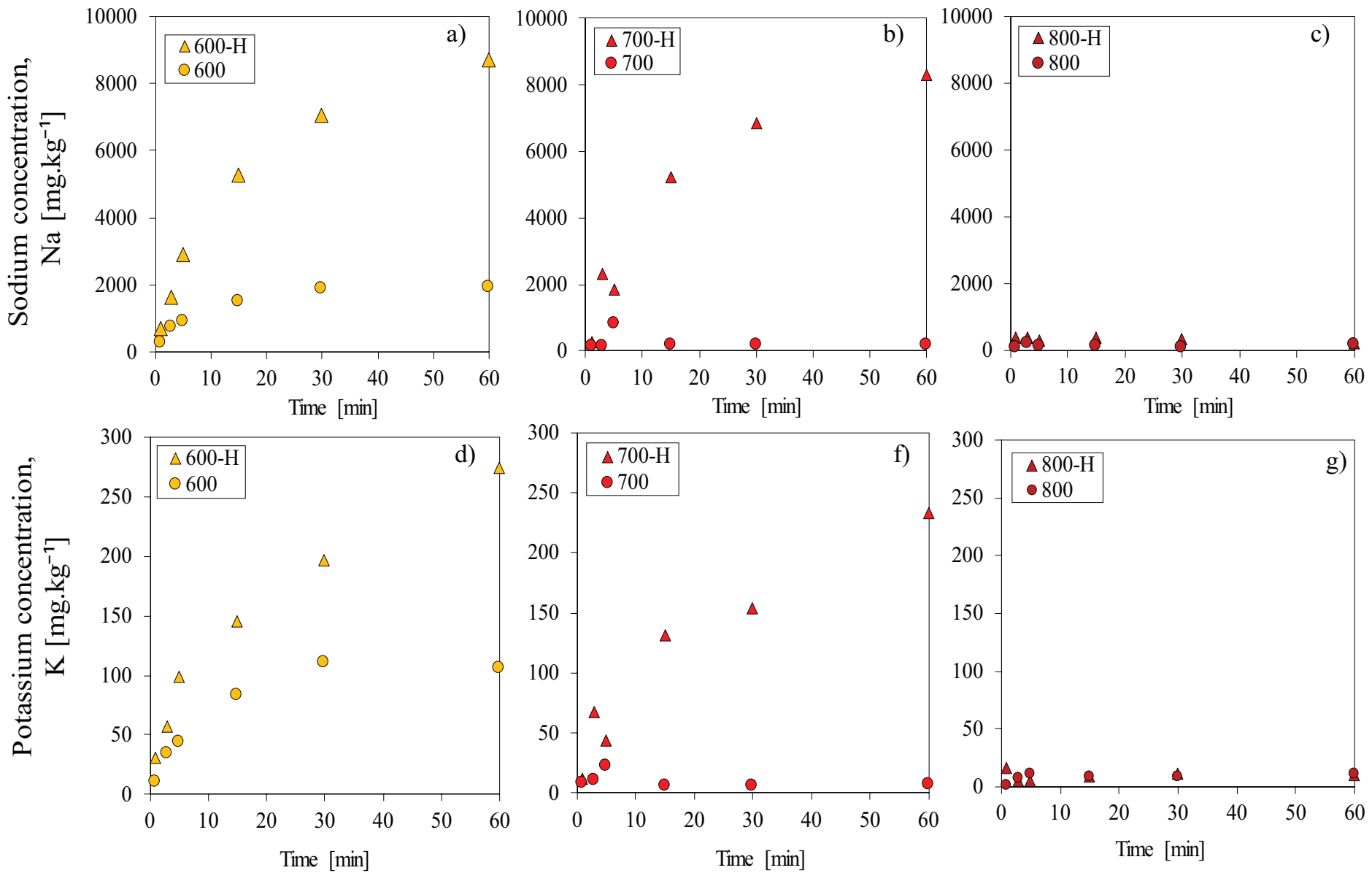

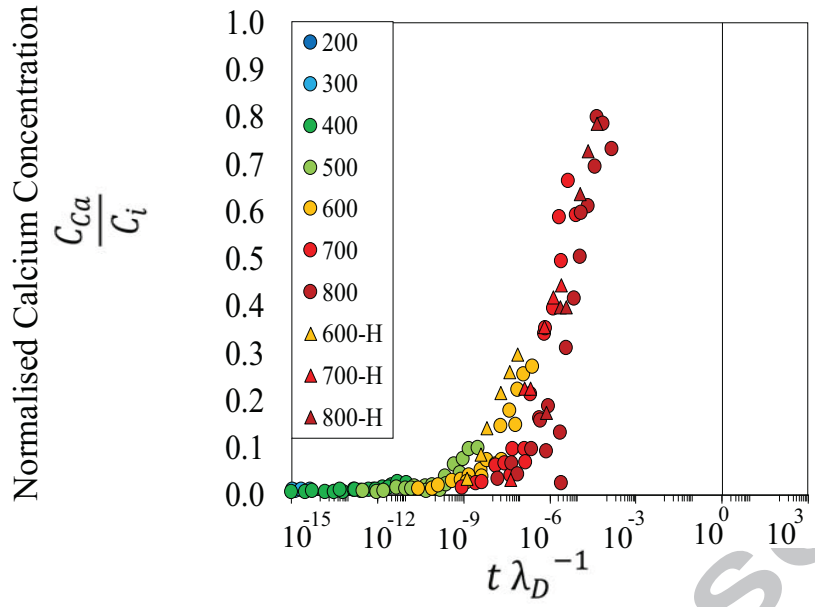

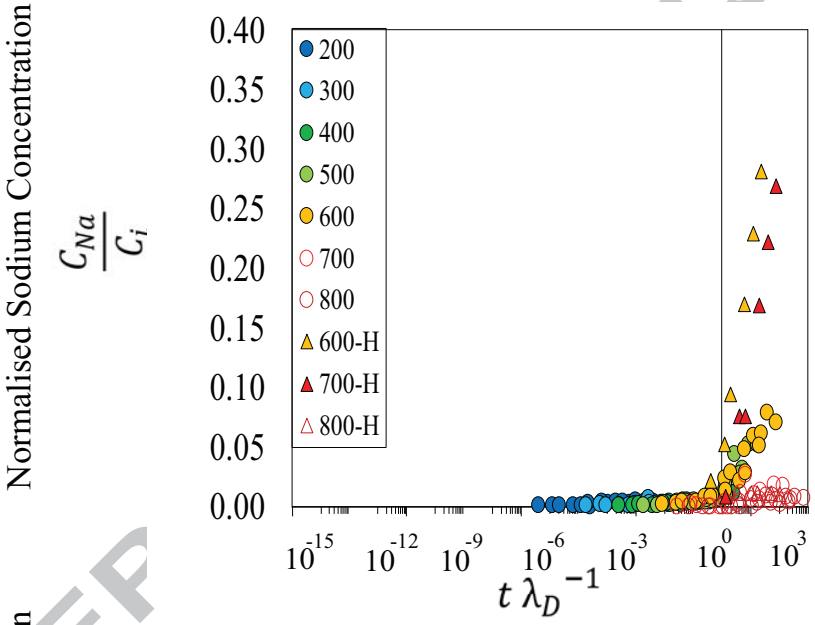

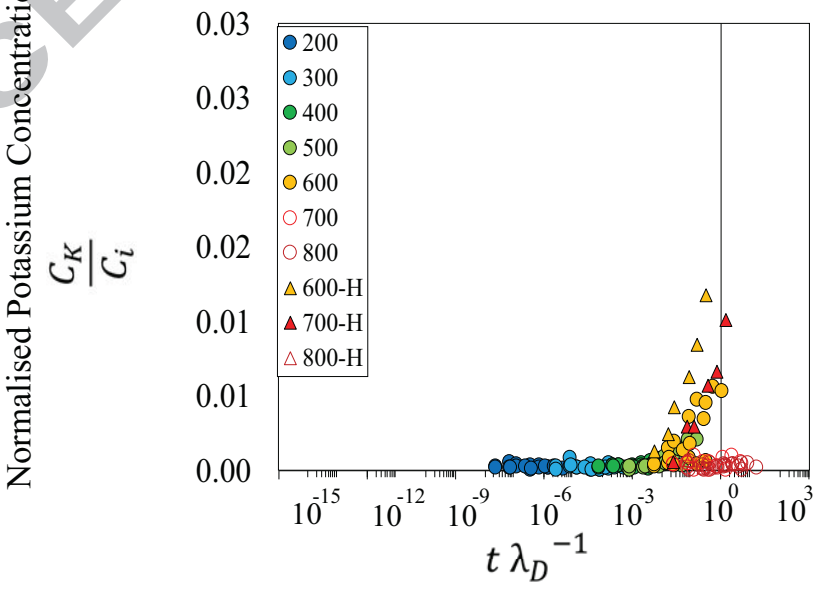

Figure 9

Tables

Table 1. Bulk chemical composition of the sample material

Element	Mean wt.%	St. dev.
SiO_2	*75.23*	*1.05*
TiO_2	*0.23*	*0.02*
Al_2O_3	*12.00*	*0.24*
FeO_T	*3.28*	*1.34*
MnO	*0.11*	*0.04*
MgO	*0.10*	*0.02*
CaO	*1.66*	*0.16*
Na_2O	*4.15*	*0.23*
K_2O	*2.75*	*0.10*
Total	*99.50*	*0.73*

Table 2. Specific surface area (Ssa) and geometric surface area (Gsa) of the sample material

Sample	Ssa (m^2g^{-1})		Gsa (m^2g^{-1})	
	Mean	St. dev	Mean	St. dev.
>90 µm	*0.26*	*0.02*	*0.04*	*0.002*
63-90 µm	*0.64*	*0.02*	*0.28*	*0.01*
<63 µm	*0.88*	*0.01*	*0.37*	*0.004*

Table 3.Characteristic leachate data (see Supplementary Datat for full dataset)

Material	Concentrations of leached cations (mg/kg)			Initial redox state of Fe	Redox state after exposure to SO2 at 800 C for 60 minutes
	Ca	Na	K	$Fe^{3+}/\Sigma Fe$	$Fe^{3+}/\Sigma Fe$
Original powdered glass	*2642.147*	*1897.366*	*105.451*	*0.153*	*0.318*
Pre-heated powdered glass	*827.817*	*308.676*	*9.111*	*0.416*	

Table 4. Published inputs to diffusion scaling

Element	D_0 ($m^2.s^{-1}$)	b (K)	Data source
Ca	2.54×10^{-5}	29830 ± 4356	Mungall et al., (1999)
Na	1.34×10^{-6}	10210 ± 243	Jambon (1982), Magaritz and Hoffmann (1978) and Watson (1981) in agreement with Zhang et al. (2010)
K	3.48×10^{-7}	12775 ± 927	Jambon (1982) in agreement with Zhang et al. (2010)